Nanoscale

PAPER

View Article Online
View Journal | View Issue

Cite this: *Nanoscale*, 2026, **18**, 2030

Ultrafast dynamics of relaxation in well-dispersed quantum-confined nanographenes

Sébastien Quistrebert, [a] Daniel Medina-Lopez,[b] Cynthia Banga-Kpako,[b] Thanh Trung Huynh,[a] Stéphane Campidelli, [b] Jean-Sébastien Lauret [a] and Elsa Cassette *[a]

Received 15th September 2025,
Accepted 9th December 2025

DOI: 10.1039/d5nr03896k

rsc.li/nanoscale

Recently developed graphene quantum dots (G-QDs), presenting exceptional dispersion stability, a precisely controlled number of conjugated carbon rings and a photoluminescence quantum yield of almost unity, allow scrutinization of their intrinsic photophysics and potential quantum-confined effects related to their excited-state dynamics. Here we use transient absorption with 30–40 fs resolution to probe electronic relaxation in rectangular G-QDs composed of exactly 96, 114 and 132 carbon atoms. Through the growth of excited-state emission signals over the ground-state bleaching ones, the dynamics of relaxation are unveiled. The relaxation time ranges between 130 and 180 fs, which leads to a maximum global energy-loss rate of 5 eV ps^{-1}. Energy-selective excitation measurements show that this ultrafast relaxation rate is limited by vibrational relaxation rather than the internal conversion process. This reveals the proximity between the excited-state energy surfaces and the key role of high-frequency vibrational modes in driving these ultrafast relaxation dynamics.

Introduction

Graphene nanostructures, such as zero-dimensional (0D) graphene "quantum dots" (G-QDs), 1D graphene nanoribbons (G-NRs) and 2D graphene nanoflakes/nanosheets (G-NFs/G-NSs), have gained attention over the past few years, notably thank to the recent developments in their synthetic methods through bottom-up approach.[1] Nanographenes combine the unique mechanical and electronic transport properties of sp^2-hybridized carbon materials, with the great optical properties of direct bandgap semiconductor materials. Their direct gap arises from the reduction of dimensionality in the 2D plane to the nanoscale and can be precisely tuned in the visible to near-infrared range with great control over their lateral sizes (*i.e.* delocalization length), shape (*i.e.* symmetry) and edge structure (zigzag *versus* armchair).[1–3]

Chemical development of large polycyclic aromatic hydrocarbons (PAHs) or strongly asymmetric carbon sp^2-based molecules, such as long acenes, has been hampered by their strong tendency to aggregate through π-stacking interactions. On the one hand, chemically stable and well-defined developed PAHs typically can only have a limited number of conjugated carbon rings (<10). The optical transitions of such PAHs are then in the blue or ultraviolet (UV) range, unless they possess charge transfer (CT) character, which is common for functionalized PAHs presenting some zigzag edges (*e.g.* TIPS-pentacenes,[4] dibenzo[*hi*,*st*]ovalenes,[5] [*m*,*n*]*peri*-acenoacenes[6]). On the other hand, the aggregation of large PAHs (nanographenes, >1 nm or composed of several tens of carbon rings) limits the purification steps due to the lack of solubility. This prevents the single population of a structure from being selectively obtained and prevents the isolation of the desired nanostructures from the precursors. Furthermore, uncontrolled π–π stacking results in large intermolecular electronic coupling that directly affects the optical properties of the nanostructures, broadens the linewidth of the optical transitions and also results in partial CT character (discussed below). In some cases, the photoluminescence (PL) properties remain more "intrinsic" to the monomers, since the PL quantum yield drastically decreases in the aggregated state,[7] but the absorption spectrum of G-QD and G-NR samples in solution are typically dominated by the aggregates.[8–10]

Overall, studying the intrinsic dynamics of the excited states in nanographenes is thus a major challenge when based on absorptive methods such as transient absorption (TA). Furthermore, CT character prevents the investigation of the fundamental effects of quantum confinement in such dynamics (modification of rate and possible concurrent mechanisms). In several studies, TA spectra of nanographenes are dominated by a broadband photoinduced absorption (PIA) signal in the visible range, for which the origin remains

[a]*Université Paris-Saclay, ENS Paris-Saclay, CNRS, CentraleSupélec, LuMIn, 91405 Orsay, France. E-mail: elsa.cassette@ens-paris-saclay.fr*
[b]*Université Paris-Saclay, CEA, CNRS, NIMBE, LICSEN, 91191 Gif-sur-Yvette, France*

unclear.[8,11–14] While several narrowband excited-state absorption (ESA) signals from the lower singlet excited state to higher-energy singlet states ($S_1 \rightarrow S_n$) might be involved, ESA from triplet states ($T_1 \rightarrow T_n$) and/or from charge (transfer) states ($C_1 \rightarrow C_n$ or $CT_1 \rightarrow CT_n$) might prevail in the origin of such broadband PIA signals.[15] Indeed, in a theoretical work, F. Spano and coworkers showed that aggregation can accelerate the rate of intersystem crossing (ISC) from singlet to triplet state, k_{ISC}, but also k_{CT}, the transfer from singlet to CT states.[16] While ESA signals involving triplets are typically observed in the near-infrared (NIR) range, (photoinduced) absorption signals from charge states or CT states should rise in the visible range and are expected to be intrinsically spectrally broad due to the continuum of energies available for these states. For instance, PAH molecules with zigzag edges presenting a strong CT character (NIR PL spectrum with relatively low number of conjugated carbon rings) and well-defined optical transitions display such large PIA signals in the visible.[6]

To limit the aggregation induced by π–π stacking, nonlinear, bulky side chains have been added chemically at the periphery of large PAHs,[9] G-QDs[17] and G-NRs.[18] In particular, the rectangular G-QDs recently synthesized by Medina-Lopez *et al.*, with armchair edges and *tert*-butyls (*t*Bu) at specific positions, display promising characteristics: the PL and absorption properties are governed by the individual nanostructures (monomers), their lateral sizes and overall structure can be precisely tuned, the excitation is delocalized and the emission energy can be directly controlled by the number of conjugated carbon rings.[17] This allows reaching fast emitters in the red and NIR range (typical lifetime of a few nanoseconds), without CT character.

In order to gain more insight into the photophysics of these nanostructures and related systems, it is of importance to study their excited-state dynamics using ultrafast optical spectroscopy. Here we use femtosecond transient absorption (fs-TA) to investigate the dynamics of relaxation of hot excited species, *i.e.* generated though excitation energy well above the gap. We investigate the underlying mechanism resulting from the fast electronic relaxation in these well-dispersed samples, with the effect of the QD length (quantum confinement) and through energy-selective excitation.

Results and discussion

The studied G-QDs were synthesized through the bottom-up approach previously described by Medina-Lopez *et al.*[17] We focused on the C_{96}-tBu$_8$ ('C96'), C_{114}-tBu$_{10}$ ('C114') and C_{114}-tBu$_{12}$ ('C132') nanostructures, where the number after the "C" refers to the exact number of sp^2 carbon atoms forming the main structure (*i.e.* without the *tert*-butyl groups). The G-QDs are respectively 2.30, 2.71 and 3.11 nm long, while retaining the same width (0.96 nm). The increase of excited-state delocalization with the QD length is observable with the low-energy shift of their optical transitions (electronic and vibrational replica) in the linear absorption and photoluminescence spectra, Fig. 1. In particular, the energy of the first electronic transition, $S_0 \rightarrow S_1$, scales as the inverse of the number of carbon atoms (Fig. S1a in the SI). This delocalization has been correlated with a decrease of the radiative lifetime[19] (Fig. S1b and discussion in the SI), which is characteristic of a giant oscillator strength for the emission transition. The absence of

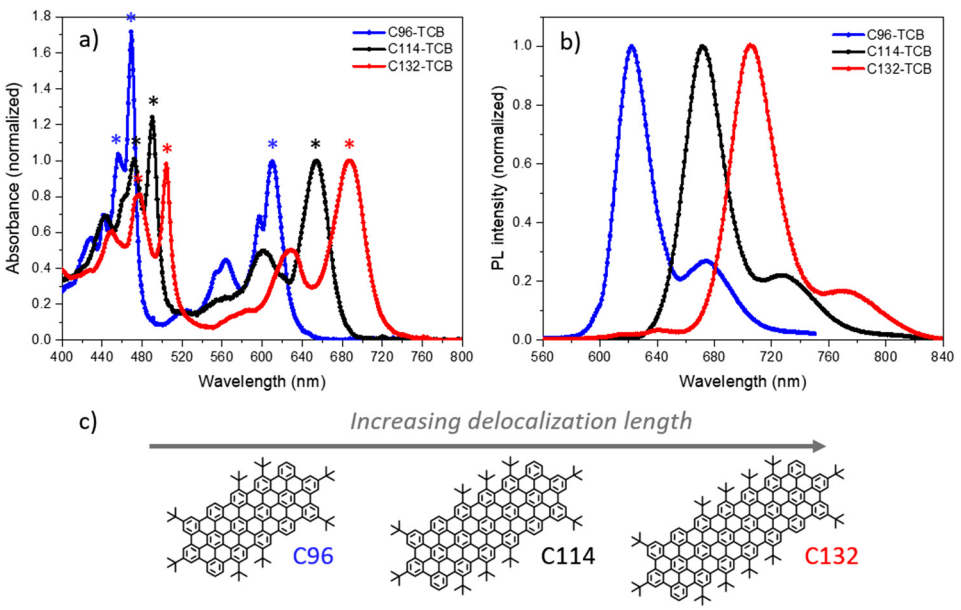

Fig. 1 Steady-state absorption (a) and PL (b) spectra of C96, C114 and C132 rectangular G-QDs dispersed in 1,2,4 trichlorobenzene (TCB), represented in blue, black and red, respectively. The spectra are normalized at the first optical transition for comparison. The G-QD spectra are composed of several electronic transitions (identified with stars) and their vibrational replicas. The corresponding chemical structures are displayed in (c).

notable CT character is discussed in the SI, by comparing the steady-state absorption and photoluminescence spectra of C114 G-QDs in different solvents (Fig. S2).

We started by investigating the dynamics of C114 G-QDs with fs-TA within the first few picoseconds. We tune the pump pulse energy to selectively excite the second optically active electronic transition of the system, which is the $S_0 \rightarrow S_5$ optical transition.[17] The differential absorption, ΔA, was measured over the visible spectral range 440–760 nm, with a temporal resolution of about 30–40 fs (see the Experimental section and Fig. S3 in the SI). This allows us to investigate the dynamics of relaxation from S_5 to S_1. Typical TA results are shown in Fig. 2, with the full TA map $\Delta A(\lambda,t)$, time-dependent TA spectra $\Delta A_t(\lambda)$ and time traces at selected wavelengths $\Delta A_\lambda(t)$. Overall, ΔA is rather negative. The strong ΔA signals at energies corresponding to the optical transitions of the steady-state absorption can be assigned as ground state bleaching (GSB) signals, related to a decrease of absorption induced by the pump pulse. A change in the TA spectra is observable during the first 200 fs: a negative signal grows at the low-energy side of the $S_0 \rightarrow S_1$ GSB signal (around 660 nm for C114 G-QDs in tetrahydrofuran, THF) and the TA signal changes from positive to negative around 725 nm. We note that an extra signal is present during the pump–probe pulse overlap, which is due to the non-resonant solvent response and not further discussed. No amplitude nor spectral changes can be observed from 0.4 to 2 ps. In the following, we show that the measured dynamics within the first hundreds of femtoseconds are related to the S_5 to S_1 electronic relaxation.

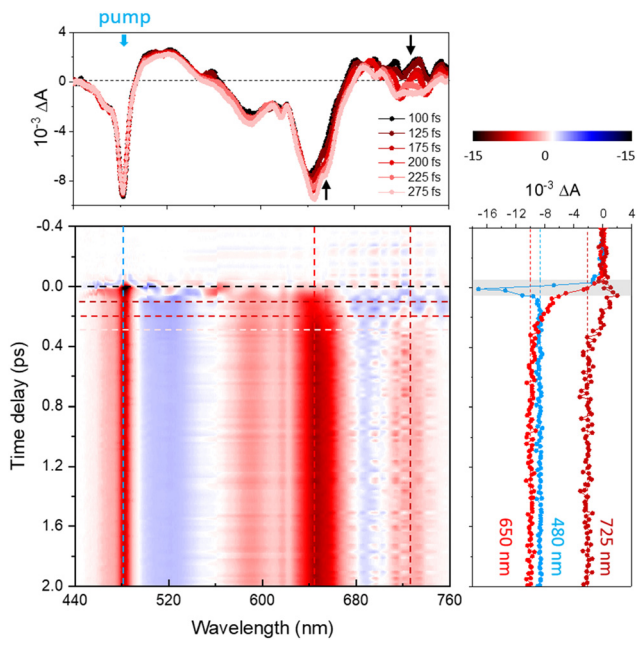

Fig. 2 TA map, TA spectra (top) and TA time traces (right side) of C114 G-QDs dispersed in tetrahydrofuran (THF), after excitation at the $S_0 \rightarrow S_5$ transition at 482 nm (blue dashed line). The measurements were made with the pump and probe vertically polarized (VV, parallel). The time during the pump–probe pulse overlap is shown, for reference, by a grey window in the decay traces.

As several TA signals might spectrally overlap, especially close to the "band edge", we perform global analysis with Glotaran, using a sequential model.[20] The global analysis in this time range leads typically to the initial (EAS_1, in black) and final (EAS_2, in pink) TA spectra Fig. 3a. The polarization of the pump (vertical, V or horizontal, H) only modifies the relative amplitude of the different optical transitions related to a specific transition dipole moment, which is perpendicular between $S_0 \rightarrow S_1$ and $S_0 \rightarrow S_5$[17] (see inset Fig. 3a). In this sequential model, EAS_1 appears with the pump pulse and its amplitude decays exponentially with a rate $k_1 = 1/\tau_1$, while EAS_2 grows with the same rate, k_1, and eventually decays with a second characteristic rate $k_2 = 1/\tau_2$. Here, τ_2 is much longer than the time range of the experiments (constant signal amplitudes within the first 2 ps), and as such we focus on the first kinetics related to k_1.

The main difference between EAS_1 and EAS_2 lies in the red part of the spectra: the EAS_2 displays extra negative features around 660 and 720 nm. These two wavelengths correspond to the two maxima of intensity of the steady-state PL spectrum (top of Fig. 3a, dashed line). Thus, these extra TA signals can be attributed to excited-state emissions (ESE), from the stimulated emissions of $S_{1,\nu'=0} \rightarrow S_{0,\nu=0}$ and $S_{1,\nu'=0} \rightarrow S_{0,\nu=1}$, schematized in the wine arrows in Fig. 3c. Importantly, these ESE signals at the PL peak energies can only be observed when the S_1 excited state is populated. When exciting directly at the first transition $S_0 \rightarrow S_1$, the ESE signals appear instantaneously (≤25 fs), as with the GSB ones, as seen in the time traces (Fig. 4b). Thus, the resolved growth of the amplitude of the ESE signals in time (Fig. 4a) corresponds to the dynamics of electronic relaxation from S_5 to S_1. The absence of change in the GSB signals (only the coherent artefact from the non-resonant solvent response is seen in the first tens of femtoseconds, *i.e.* during the pump and probe pulse overlap) is consistent with a molecular system that cannot accept more than one excitation: the reduction of absorption of the different optical transitions is similar either the S_5 or S_1 state is populated (schematics Fig. 3b). The relaxation from S_5 to S_1 can also involves changes of excited-state absorption (ESA) signals to higher-energy states, such as $S_5 \rightarrow S_n$. For instance, a positive signal is slightly evolving around 500–525 nm and another is initially present around 670–760 nm. These changes are also taken into account with the global fit.

In terms of relaxation time, τ_1, the fit of the TA results of C114 in THF gives initially 160 ± 5 fs (batch 1, Fig. 3a and 4a, standard deviation over three measurements). We found a slightly faster relaxation time, 130 ± 5 fs (standard deviation over four measurements), in more recent experiments performed on another G-QD sample (batch 2, Fig. S4a in the SI). Particular care should be taken in the global fit to properly adjust the dispersion of the probe pulse (wavelength-dependent time zero, see Fig. S3a in the SI), since the growing ESE signal at the maximum PL position overlaps with the quasi-instantaneously rising GSB one. We also performed the same

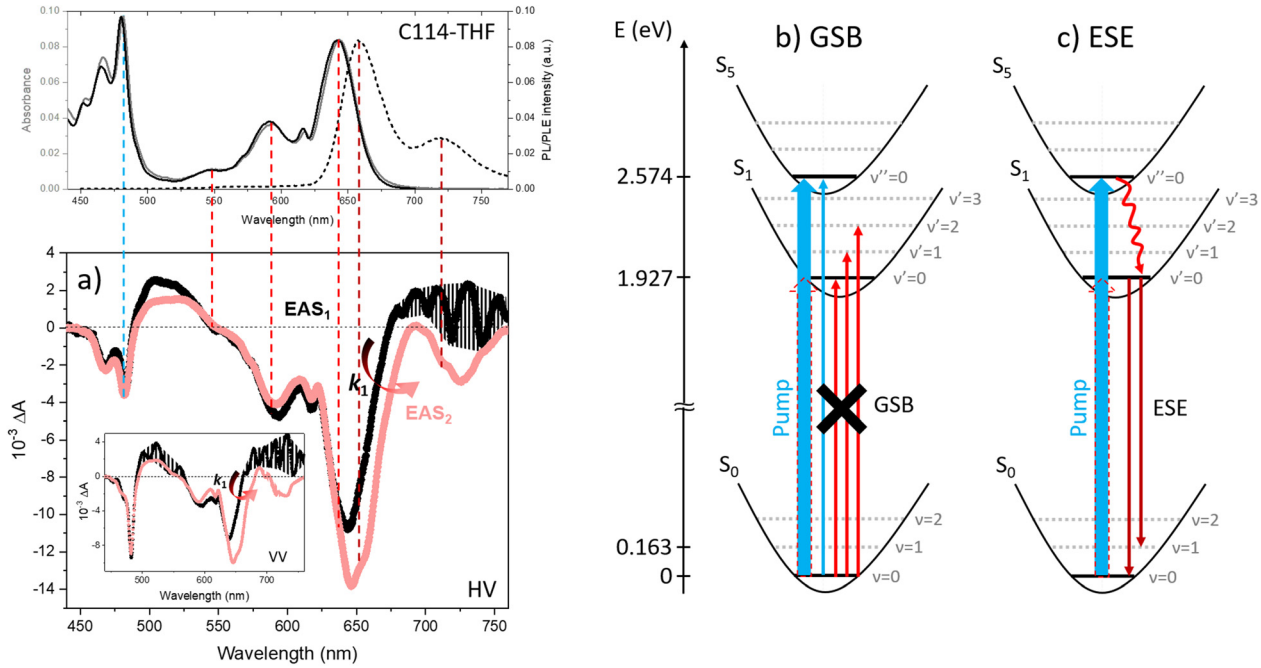

Fig. 3 (a) Initial (EAS_1, black) and final (EAS_2, pink) evolution associated spectra obtained from a global analysis of the TA data of C114 G-QDs in THF, after excitation at the $S_0 \rightarrow S_5$ transition (at 480 nm, blue dashed line), in parallel (VV) and perpendicular (HV) excitation–detection polarization configurations. The dashed areas are added to visualize the pulse-to-pulse spectral fluctuations of the continuum probe. The steady-state absorption (black line), PL (dashed line) and PL excitation (PLE, grey line) spectra are shown in the top panel in order to correlate the TA signals with the different optical transitions. The global fit gives $\tau_1 = 1/k_1$ of 155 fs and 163 fs for the VV and HV configurations, respectively. (b) and (c) Simplified schematic diagrams of the electronic (full lines) and vibrational (dot lines) energy levels and the origin of the ground-state bleaching (GSB) and excited-state emission (ESE) signals. The electronic states are labelled as S_n (n = 0 for ground state, n = 1, 5, 10 for the different bright excited states[17]), while the vibrational quanta corresponding to the C–C stretching mode are numbered as $\nu/\nu'/\nu''$ = 0, 1, 2, 3, *etc*.

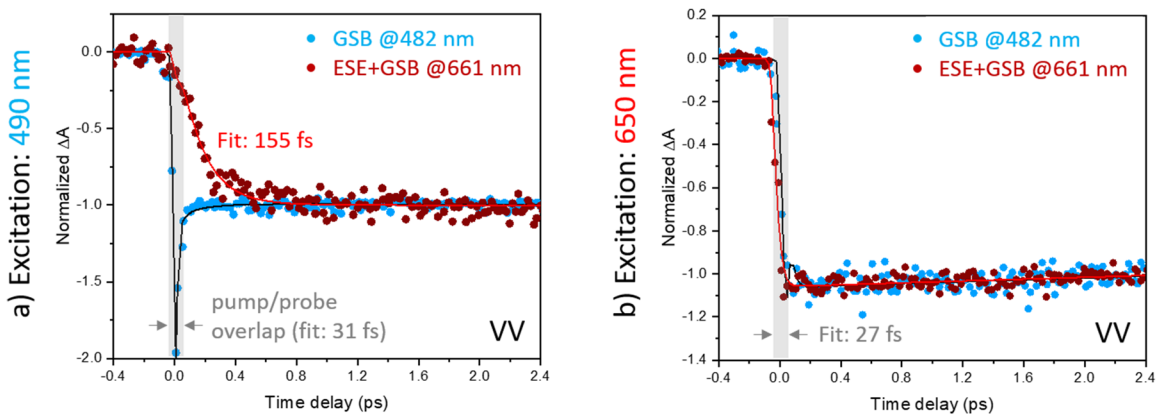

Fig. 4 (a) and (b) Experimental time traces (dots) and fits (lines, from global analysis) at selected wavelengths for measurements of C114 G-QDs with excitation corresponding to the $S_0 \rightarrow S_5$ and $S_0 \rightarrow S_1$ transitions, respectively. The time traces are normalized to –1 at long time.

experiment for C114 G-QDs dispersed in 1,2,4-trichlorobenzene (TCB), within a flow cell in order to limit any photostability issue. The excitation at the $S_0 \rightarrow S_5$ transition (490 nm for C114 in TCB) leads to similar but slightly longer relaxation times of 180 ± 3 fs (batch 1) and 147 ± 10 fs (batch 2, Fig. S4b in the SI). The results are recapitulated in Fig. S4c in the SI.

As electronic relaxation is a complex process that can involve different steps and mechanisms, TA experiments up to a few nanoseconds were performed to ensure that the full relaxation dynamics have occurred within the first few hundreds of femtoseconds, related to the k_1 kinetics. For instance, inter-molecular vibrational energy transfer with the solvent molecules can take place in the range of several picoseconds. The results are presented in the SI (Fig. S5). Apart from the rotational diffusion of the G-QDs in the solution that is observed with the polarization-dependent experiments in

several hundreds of picoseconds, another dynamic process is further observed in the range of a few nanoseconds, and corresponds well to the $S_1 \rightarrow S_0$ recombination measured in time-correlated single photon counting (TCSPC, Fig. S1b). Thus, the sub-200 fs dynamics cover the full electronic relaxation process from $S_{5,\nu'=0}$ to $S_{1,\nu=0}$, which corresponds to a global energy-loss rate of about 3.5–4.3 eV ps^{-1} in TCB and 4–5 eV ps^{-1} in THF. The consistent shorter dynamics observed in the G-QDs from batch 2 relative to batch 1 might be related to some limited aggregation effect in this sample, favoring extra nonradiative relaxation processes (*cf.* Introduction). For instance, we did notice a slight shortening of the relaxation time of a few tens of fs when the measurements were performed on aged solutions of G-QDs. That is why we performed the measurements on freshly dispersed nanographenes (the same day or the day before). With the relaxation dynamics from S_5 to S_1 in C114 G-QDs being characterized, we then turned to the mechanism behind this process.

We performed fluence-dependent experiments up to almost 1 mJ cm^{-2}. The results are displayed in Fig. S6a–c in the SI and lead to very similar relaxation times (C114 G-QDs in THF, batch 2). This is in contrast with the hot phonon bottleneck and Auger reheating effects observed in inorganic two-dimensional systems, where the relaxation dynamics can be delayed to more than one order of magnitude due to the proximity of the excited species.[21–23] In particular, the amplitude decays over long times (picoseconds to nanoseconds) are not affected at large excitation fluence, which shows the absence of multi-excited-state dynamics such as exciton–exciton annihilation (Fig. S6d in the SI). This further confirms that the rectangular C114 G-QDs still behave like "zero-dimensional" systems, despite their relatively large size. We thus expect a mechanism of relaxation similar to the one in PAH molecules.

Full relaxation in molecular systems classically involves an internal conversion process (IC) followed by intra- (and inter-) molecular vibrational relaxation (VR) ones. The first step, IC, is an iso-energetic process allowing the conversion of energy between a highly excited electronic state $S_{n,\nu''=0}$ ($n > 1$) to a lower excited state with a large number of vibrational quanta, $S_{1,\nu'=m}$ ($m > 0$). VR instead does not involve a change of electronic state of the structure, but corresponds to the dissipation of vibrational energy through heat, by redistribution to other, low-energy, vibrational modes within (or outside) the structure.[24] Classically, IC is much slower than VR and its rate is calculated based on a derivation from Fermi's golden rule, as a product of an electronic term characterizing the vibronic coupling between the two electronic states, by the Franck–Condon (FC) factor (square of the overlap integral of the vibrational wavefunctions).[25,26] As the energy to relax increases, the FC factor decreases, resulting in a slower IC rate (energy-gap law, schematized in Fig. S9a in the SI). However, in some cases, due to the proximity of the bright and dark states within the excited-state manifold, and non-harmonicities in the potential energy surfaces, the Born–Oppenheimer approximation may break down (*i.e.* regime of strong vibronic coupling), leading to nonadiabatic relaxation processes. This results in deviation from classical IC rates and mechanism, with for instance a pathway mediated by conical intersections (as illustrated in Fig. S9b in the SI).

To gain insight into the mechanism of the fast relaxation in our G-QDs, we investigated the effect of the QD length (quantum confinement) on the electronic relaxation rate by measuring the experimental relaxation in the shorter C96 and longer C132 G-QDs. The equivalent electronic transition for the pump excitation in C96 (C132) is called $S_0 \rightarrow S_4$ ($S_0 \rightarrow S_6$)[17] and its energy is 2.63 eV (2.46 eV) in TCB (corresponding to 471 nm and 504 nm, respectively, in the absorption spectrum Fig. 1a). The first allowed electronic transition, $S_0 \rightarrow S_1$ (at 612 nm for C96, 688 nm for C132), is more affected in energy by the excited-state delocalization than the second one,[17] such that the overall difference in energy between the two first bright electronic states increases from $\Delta E = 0.608$ eV in C96, to $\Delta E = 0.634$ eV in C114, and further to $\Delta E = 0.658$ eV in C132. Thus, following the classical energy-gap law, one could expect the relaxation time to increase with the NG length.[25]

The TA data for the C96 G-QDs in TCB, after excitation at the $S_0 \rightarrow S_4$ transition, are shown in Fig. S7 in the SI. We found a relaxation time of 157 ± 3 fs. This is slightly shorter than the dynamics measured in batch 1 of C114 in TCB (180 fs) but similar to the results for batch 2, which might involve some intermolecular coupling effects. The synthesized C96 samples are well-solubilized in TCB, and always display some single photon source properties at low density in matrices or on substrate, as reported in our research group.[27] It was, however, more difficult to measure the dynamics of the C132 G-QDs in TCB due to increased instability issues at the concentrations we used for TA measurements (typical optical density of 0.25 with a cuvette path length of 1 mm). Moreover, the TA spectra are much less stable in the range of the PL emission due to the large fluctuations of the probe spectrum (Fig. S8a). The relaxation times for this sample varies from 150 fs to 190 fs, with a mean value of 173 fs (standard deviation 20 fs, see Fig. S8d in the SI). Given the dispersion and the relatively small variation in the relaxation time from sample to sample compared to the experimental standard deviation for each population of G-QD, we directly compared the TA time traces at the maximum PL peak for each sample (Fig. S8b–d). The dynamics overlap, such as no size effect could be evidenced on the relaxation dynamics. We should however note that both ESE and instantaneous GSB are contributing at these wavelengths.

The measured relaxation dynamics deviate from the classical energy-gap law, with the absence of correlation between energy and QD length. This is even more striking when comparing the relaxation rate of C114 in the two solvents: k_1 is consistently larger in THF than in TCB, while the energy difference between S_5 and S_1 is larger. It is known that the difference of polarity between solvents typically affects the intermolecular vibrational relaxation process, but this typically takes place in the range of 1–100 picoseconds and can be resolved as a spectral shift of the ESE signals.[28] Such a dynamic Stokes shift is not observed for our G-QD systems

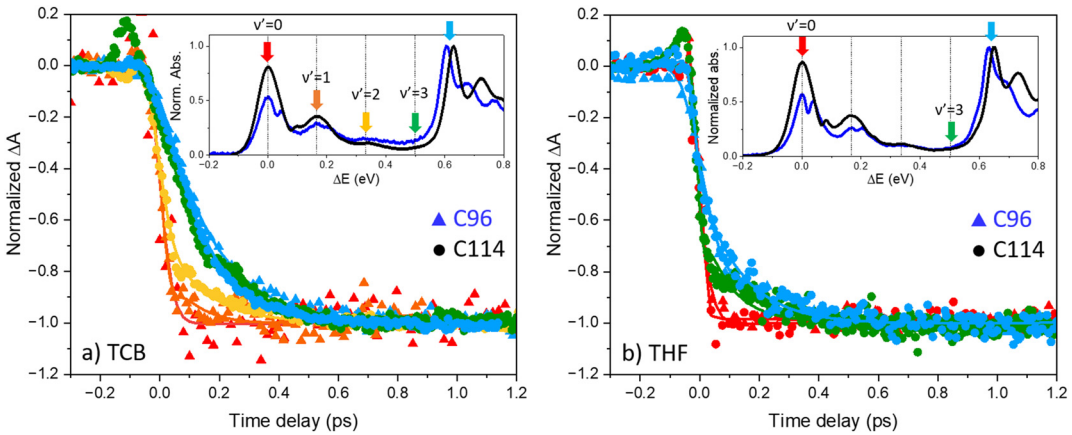

Fig. 5 Time traces at the maximum PL energy showing the growth of the ESE signals for C96 (triangles) and C114 (dots) G-QDs dispersed in TCB (a) and in THF (b). The colors of the traces correspond to the selected excitation wavelengths corresponding to the "band edge" $S_0 \rightarrow S_1$ (red), its different vibrational replicas (yellow, orange and green), as well to the $S_0 \rightarrow S_{5/4}$ transition for comparison (blue). The fits (from global analysis) are displayed as solid lines. The positions of the excitation wavelengths are illustrated in the linear absorption of the samples shown in the insets, with the horizontal axis showing the excess energy relative to the first transition. The results of the fit are given in Table S1 in the SI.

during the first hundreds of femtoseconds, nor at longer times. Nevertheless, the solvent can modify the configuration of the excited states in the G-QDs, affecting the Franck–Condon factors[29] and electronic couplings, and/or might activate some vibrational modes. Here, the relatively small difference between the experimental relaxation dynamics of C114 G-QDs in THF compared to those in TCB does not specially emphasize the role of an additional activated vibrational mode. Moreover, similar vibrational modes are observed in the linear absorption spectrum, between S_0 and S_1 and between S_0 and S_5 (Fig. S10).

With increasing the QD length, we also increase the density of potential energy surfaces for all excited states (bright and dark), favoring their vibronic coupling and potential intersections. We should note that the experimental data and global analysis do not evidence any signature of the contribution of intermediate dark states in the relaxation process between the first two bright electronic states. The relaxation time is similar for the G-QD samples of different lengths, whereas the number of intermediate dark states increases from two in C96 to three in C114, to four in C132. The measured relaxation dynamics are systematically ultrafast given the relatively large energy to dissipate but still slower than the typical expected dynamics involving nonadiabatic processes with conical intersections (in the tens of fs). In the following we show that the IC step is actually ultrafast (<100 fs) and that the dynamics are rather limited by the vibrational relaxation step.

We investigated the dynamics of vibrational relaxation by selectively exciting our samples at given replica corresponding to the C–C stretching vibrational mode at around 1310–1335 cm^{-1} or 163–166 meV (*cf.* schematic diagrams in Fig. 3b and c and defined transitions in Fig. S10 in the SI). The high frequency of the C–C stretching modes in π-conjugated molecules combined with their relatively large Huang Rhys factor (see Fig. S10 in the SI) are known to contribute efficiently to fast relaxation. The excitation at the band edge, 610 nm for C96 in TCB (Fig. 5a, red triangles) and respectively 595 and 650 nm for C96 and C114 G-QDs in THF (Fig. 5b, red dots/triangles), leads to the apparition of an "instantaneous" (*i.e.* within our temporal resolution) ESE signal at the energy of the PL maximum. However, the excitation at increasing quanta of the vibrational replica results in the progressive slowing down of the dynamics (orange, yellow and green data points in Fig. 5), until it almost reaches the one measured when exciting at the $S_0 \rightarrow S_5$ transition (blue dots/triangles). For instance, in Fig. 5a, the dynamics of relaxation of C114 G-QDs (batch 2) in TCB increases to 112 fs for excitation at $S_0 \rightarrow S_{1,v'=2}$ (559 nm, yellow dots) and further to 144 fs when exciting at $S_0 \rightarrow S_{1,v'=3}$ (505 nm, green dots). The recapitulative results for the fits are displayed in Table S1 in the SI. Importantly, they show that the full electronic relaxation from S_n to S_1 is limited by the VR process.

Experimental methods

Steady-state optical characterizations and TR-PL

Absorption spectra were recorded with a UV–visible commercial spectrophotometer (Lambda 950, PerkinElmer), in a quartz cuvette with an optical path of 1 mm or 1 cm. Photoluminescence (PL) and photoluminescence excitation (PLE) spectra were measured using a commercial fluorimeter (FS5, Edinburg Instrument) in a 1 cm quartz cuvette. PL quantum yields were previously measured with the integrated sphere (SC-30), for excitation at the second allowed electronic transition. Fluorescence anisotropy in excitation was measured by acquiring PLE spectra in the four following polarization configurations: ij = VV, VH, HV and HH. The anisotropy factor is given by:

$$R = \frac{I_{VV} - GI_{VH}}{I_{VV} + 2GI_{VH}},$$

where I_{ij} is the fluorescence intensity for a specific polarization configuration in excitation (i) and detection (j), and G is the

factor which corrects from the difference of detection sensitivity in the vertical and horizontal polarizations $\left(G = \frac{I_{HV}}{I_{HH}}\right)$. TR-PL was measured on the same fluorimeter (detector response <0.5 ns), using a pulsed laser diode at 405 nm (EPL-405 nm) as the excitation source.

Femtosecond transient absorption (fs-TA)

Experiments were carried out at room temperature in a 1 mm thick quartz (flow) cell. Sample solutions were prepared with an optical density of about 0.2–0.25 within the detection range (440–760 nm). The sample solutions were freshly prepared (QD solubilization in the solvent) and filtered prior to measurement (0.2 μm pores). When TCB was used as the solvent, the solution was recirculated by connecting our flow cell with a peristaltic pump. The homebuilt fs-TA setup is based on an amplified TiSa laser source (800 nm, 80 fs, 4 kHz, >6 W, Astrella, Coherent). The pump was tuned in the visible range according to the selected optical transition with a homemade non-collinear optical parametric amplifier (NOPA) and chopped at 2 kHz. For the probe, we generate the white light (WL) continuum (440–760 nm) with a 2 mm thick sapphire plate. The WL transmitted through the sample was dispersed with a spectrograph and the intensity spectrum $I(\lambda)$ was recorded at 4000 fps (shot-to-shot) using a CCD camera (ProEM-HS 1024, Princeton Instrument, binning over the 64 first vertical pixels). The pump and probe pulses were compressed with chirped mirror pairs (Layertec, −25 fs^2 per bounce, 13 bounces for the pump, 8 for the WL). The temporal resolution of the setup is about 30 fs, as estimated with the non-resonant response of the solvent (cross-phase modulation, see Fig. S3 in the SI). Global analysis of the TA results were obtain with Glotaran,[20] using a sequential model.

Conclusions

We have investigated the ultrafast dynamics of G-QDs after excitation above the bandgap, at specific electronic and vibrational transition energies. While the electronic relaxation dynamics in graphene nanostructures are often blurred by large broadband PIA/ESA signals, here the strongly limited aggregation in the studied G-QD samples allows clear observation and identification of the discrete GSB and ESE signals. The specific amplitude evolution is scrutinized with a temporal resolution of a few tens of femtoseconds. In particular, we show that the growth of ESE signals is the signature of the electronic (and vibrational) relaxation process through the population of the lower excited state S_1. The results reveal that the process of electronic relaxation is limited by the vibrational relaxation step, which is, however, ultrafast (<200 fs). The internal conversion step takes place in less than 100 fs and thus might involve a conical intersection between the excited states. While specific theoretical calculations would need to be performed to confirm this hypothesis, modifications of the G-QD nanostructures with functional groups could potentially lead to an energy barrier capable of limiting access to the conical intersection, and thus strongly delay the relaxation process. Otherwise, a rigid environment could help by reducing the internal vibrational relaxation due to coupling between the high- and low-frequency vibrational modes.

Author contributions

E. C. conceived the research project (conceptualization). D. M. L. and C. B. K. synthesized the G-QD samples under the supervision of S. C. (resources). S. Q. and E. C. performed the spectroscopic measurements and treated the data (T. T. H. provided some TR-PL data) (investigation). E. C. analysed the data (formal analysis), made the figures (visualization) and wrote the manuscript and the SI (writing – original draft). S. Q. and J. S. L. participated in the scientific discussion. J. S. L. gave input on the manuscript and all co-authors edited it (writing – review & editing). E. C., J. S. L. and S. C. provided financial support (funding acquisition).

Conflicts of interest

There are no conflicts to declare.

Data availability

The data supporting the results reported in this article can be found here: https://sdrive.cnrs.fr/s/9oy5x6ECpdnaJpC.

Supplementary information (SI): additional measurements on linear absorption and PL with eventual fit, lifetimes, TA temporal resolution, short- and long-term TA traces, EAS for C96 and C132 G-QDs, and fluorescence anisotropy. See DOI: https://doi.org/10.1039/d5nr03896k.

Acknowledgements

E. C. and J. S. L. thank David Beljonne and Silvio Osella for stimulating discussion. E. C. thanks the Agence Nationale de la Recherche (ANR) for the research grant ANR-23-CE29-0003-01, the Ecole Normale Supérieure de Paris-Saclay (ENS Paris-Saclay) and the LabEx Charmmat (ANR-11-LABX-0039) for funding. S. Q. thanks the ENS Paris-Saclay for his Masters internship and PhD funding. J. S. L. and S. C. thank the ANR (ANR-22-CE47-0001-03, ANR-21-CE09-0025, ANR-19-GRF1-0002-01) and the LabEx NanoSaclay (ANR-10-LABX-0035) for partial funding.

References

1 Y. Gu, Z. Qiu and K. Müllen, *J. Am. Chem. Soc.*, 2022, **144**, 11499–11524.
2 R. Rieger and K. Müllen, *J. Phys. Org. Chem.*, 2010, **23**, 315–325.

3 M. C. Drummer, V. Singh, N. Gupta, J. L. Gesiorski, R. B. Weerasooriya and K. D. Glusac, *Photosynth. Res.*, 2022, **151**, 163–184.
4 R. D. Pensack, A. J. Tilley, S. R. Parkin, T. S. Lee, M. M. Payne, D. Gao, A. A. Jahnke, D. G. Oblinsky, P.-F. Li, J. E. Anthony, D. S. Seferos and G. D. Scholes, *J. Am. Chem. Soc.*, 2015, **137**, 6790–6803.
5 G. M. Paternò, L. Nicoli, Q. Chen, K. Müllen, A. Narita, G. Lanzani and F. Scotognella, *J. Phys. Chem. C*, 2018, **122**, 25007–25013.
6 R. Muñoz-Mármol, F. Gordillo, V. Bonal, J. M. Villalvilla, P. G. Boj, J. A. Quintana, A. M. Ross, G. M. Paternò, F. Scotognella, G. Lanzani, A. Derradji, J. C. Sancho-García, Y. Gu, J. Wu, J. Casado and M. A. Díaz-García, *Adv. Funct. Mater.*, 2021, **31**, 2105073.
7 T. Liu, C. Tonnelé, S. Zhao, L. Rondin, C. Elias, D. Medina-Lopez, H. Okuno, A. Narita, Y. Chassagneux, C. Voisin, S. Campidelli, D. Beljonne and J.-S. Lauret, *Nanoscale*, 2022, **14**, 3826–3833.
8 M. C. Drummer, R. B. Weerasooriya, N. Gupta, B. T. Phelan, A. J. S. S. Valentine, A. A. Cordones, X. Li, L. X. Chen and K. D. Glusac, *J. Phys. Chem. C*, 2022, **126**, 1946–1957.
9 D. Wasserfallen, M. Kastler, W. Pisula, W. A. Hofer, Y. Fogel, Z. Wang and K. Müllen, *J. Am. Chem. Soc.*, 2006, **128**, 1334–1339.
10 X. Yan, X. Cui and L. Li, *J. Am. Chem. Soc.*, 2010, **132**, 5944–5945.
11 D. Sebastian, A. Pallikkara, H. Bhatt, H. N. Ghosh and K. Ramakrishnan, *J. Phys. Chem. C*, 2022, **126**, 11182–11192.
12 M. Reale, A. Sciortino, M. Cannas, E. Maçoas, A. H. G. David, C. M. Cruz, A. G. Campaña and F. Messina, *Materials*, 2023, **16**, 835.
13 M. Nazari, C. D. Bösch, A. Rondi, A. Francés-Monerris, M. Marazzi, E. Lognon, M. Gazzetto, S. M. Langenegger, R. Häner, T. Feurer, A. Monari and A. Cannizzo, *Phys. Chem. Chem. Phys.*, 2019, **21**, 16981–16988.
14 X. Chen, Z.-S. Li, H.-Y. Wang, L. Wang, Y.-Y. Yue, Y.-X. Zhang, J.-L. Du, Y. Wang and H.-B. Sun, *Opt. Mater. Express*, 2021, **11**, 3486.
15 J. Clark and G. Lanzani, *Nat. Photonics*, 2010, **4**, 438–446.
16 N. J. Hestand and F. C. Spano, *J. Chem. Phys.*, 2015, **143**, 244707.
17 D. Medina-Lopez, T. Liu, S. Osella, H. Levy-Falk, N. Rolland, C. Elias, G. Huber, P. Ticku, L. Rondin, B. Jousselme, D. Beljonne, J.-S. Lauret and S. Campidelli, *Nat. Commun.*, 2023, **14**, 4728.
18 T. Nagahara, F. V. A. Camargo, F. Xu, L. Ganzer, M. Russo, P. Zhang, A. Perri, G. de la Cruz Valbuena, I. A. Heisler, C. D'Andrea, D. Polli, K. Müllen, X. Feng, Y. Mai and G. Cerullo, *Nano Lett.*, 2024, **24**, 797–804.
19 H. Levy-Falk, Optical spectroscopy of graphene quantum dots and halide perovskite nanocrystals, PhD thesis, Université Paris-Saclay, 2024, https://theses.hal.science/tel-04429002v1.
20 J. J. Snellenburg, S. P. Laptenok, R. Seger, K. M. Mullen and I. H. M. van Stokkum, *J. Stat. Software*, 2012, **49**, 1–22.
21 C. Villamil Franco, G. Trippé-Allard, B. Mahler, C. Cornaggia, J.-S. Lauret, T. Gustavsson and E. Cassette, *J. Phys. Chem. Lett.*, 2022, **13**, 393–399.
22 E. Baghani, S. K. O'Leary, I. Fedin, D. V. Talapin and M. Pelton, *J. Phys. Chem. Lett.*, 2015, **6**, 1032–1036.
23 T. Wang, T. R. Hopper, N. Mondal, S. Liu, C. Yao, X. Zheng, F. Torrisi and A. A. Bakulin, *ACS Nano*, 2023, **17**, 6330–6340.
24 T. Kumpulainen, B. Lang, A. Rosspeintner and E. Vauthey, *Chem. Rev.*, 2017, **117**, 10826–10939.
25 J. Delaire, J. Piard, R. Méallet-Renault and G. Clavier, *Photophysique et Photochimie: Des fondements aux applications*, EDP Sciences, 1ère éditi., 2016.
26 L. Shi, X. Xie and A. Troisi, *J. Chem. Phys.*, 2022, **157**, DOI: 10.1063/5.0102857.
27 H. Levy-Falk, O. Capelle, T. Liu, D. Medina-Lopez, E. Deleporte, S. Campidelli, L. Rondin and J.-S. Lauret, *Phys. Status Solidi*, 2023, **260**, DOI: 10.1002/pssb.202370033.
28 N. Dozova, L. Ventelon, G. Clermont, M. Blanchard-Desce and P. Plaza, *Chem. Phys. Lett.*, 2016, **664**, 56–62.
29 H. Fidder, M. Rini and E. T. J. Nibbering, *J. Am. Chem. Soc.*, 2004, **126**, 3789–3794.